HAL
open science

Growth and micromagnetism of self-assembled epitaxial fcc(111) cobalt dots

Olivier Fruchart, Aurélien Masseboeuf, Jean-Christophe Toussaint, Pascale Bayle-Guillemaud

To cite this version:

Olivier Fruchart, Aurélien Masseboeuf, Jean-Christophe Toussaint, Pascale Bayle-Guillemaud. Growth and micromagnetism of self-assembled epitaxial fcc(111) cobalt dots. Journal of Physics: Condensed Matter, 2013, 25, pp.496002. 10.1088/0953-8984/25/49/496002 . hal-00857346

HAL Id: hal-00857346

https://hal.science/hal-00857346v1

Submitted on 3 Sep 2013

HAL is a multi-disciplinary open access archive for the deposit and dissemination of scientific research documents, whether they are published or not. The documents may come from teaching and research institutions in France or abroad, or from public or private research centers.

L'archive ouverte pluridisciplinaire **HAL**, est destinée au dépôt et à la diffusion de documents scientifiques de niveau recherche, publiés ou non, émanant des établissements d'enseignement et de recherche français ou étrangers, des laboratoires publics ou privés.

Growth and micromagnetism of self-assembled epitaxial fcc(111) cobalt dots

O. Fruchart*,[1] A. Masseboeuf†,[2] J. C. Toussaint,[1,3] and Pascale Bayle-Guillemaud[2]

[1] *Institut NÉEL, CNRS & Université Joseph Fourier – BP166 – F-38042 Grenoble Cedex 9 – France*
[2] *CEA-Grenoble, INAC/SP2M/LEMMA, 17 rue des Martyrs, Grenoble, France*
[3] *Grenoble - Institut National Polytechnique – France*

(Dated: September 3, 2013)

We developed the self-assembly of epitaxial submicrometer-sized face-centered-cubic (fcc) Co(111) dots using pulsed laser deposition. The dots display atomically-flat facets, from which the ratios of surface and interface energies for fcc Co are deduced. Zero-field magnetic structures are investigated with magnetic force and lorentz microscopies, revealing vortex-based flux-closure patterns. A good agreement is found with micromagnetic simulations.

I. INTRODUCTION

Physical and chemical properties are often significantly changed in low-dimensional systems, compared with materials in their bulk form. Top-down techniques based on the combination of lithography and thin-film deposition are the major approach for producing low-dimensional structures, because of the nearly unlimited freedom for designing planer shapes. Top-down techniques however reach their limits when it comes to producing complex three-dimensional systems, or features with very small sizes. For such purposes bottom-up synthesis routes, also called self-assembly, are more effective and their use has been constantly rising in the past one or two decades. Dramatic achievements have been made in both directions, with for instance porous templates such as the case of anodic alumina[1–4] or programmable architecture based on matching DNA strands[5] for complex non-flat architectures, and the fabrication of supported clusters with a size controlled down to one single atom[6].

In the field of magnetism, the use of self-assembly for its ability to produce tiny structures has brought many breakthroughs[7–9] such as: giant orbital moment and magnetic anisotropy energy at surfaces of itinerant ferromagnets[6], ferromagnetism of small Rh clusters while its bulk form is non-magnetic[10]; manipulation through electric field of the magnetic order such as antiferromagnetic Fe[11]; nanometers-sized ferromagnetic columns embedded in a non-magnetic matrix[12, 13], synthesis of artificial multiferroic metamaterials[14]. Concerning thick or even three-dimensional structures, self-assembly has been used to produce assemblies of nanowires in porous membranes[15, 16], clusters and elongated objects through chemistry[17], and dots and wires at surfaces by physical means based on dewetting processes[18–22]. The typical dimensions of such objects range from a few nanometers to a few hundreds of nanometers. At this scale one physical issue is micromagnetism (magnetization reversal and the arrangement of domains), self-assembly providing a model system.

We reported a series of micromagnetic studies based on self-assembled sub-micrometer-sized epitaxial Fe(110) dots deposited on W(110) and Mo(110) surfaces[22]. These dots are elongated owing to the (110) symmetry, and may thus display a domain wall along its length[23, 24]. These dots were thus used to observe[8] and manipulate[25, 26] the internal degrees of freedom of Bloch domain walls. The physics of magnetic vortices, the one-dimensional analogous of the two-dimensional domain walls, is also prone to a rich physics[27, 28]. This calls for the availability of self-assembled dots with a high rotational symmetry, suited for the occurrence of magnetic vortices.

Here we report the self-assembly of face-centered cubic (fcc) Co dots along the (111) orientation, with a lateral size of the order of a few hundreds of nanometers. Prior reports of self-assembled Co dots exist however with a rather flat shape and with a much smaller size so that facets cannot be identified and/or vortices do not form[29–31]. Larger dots were reported, however with no thorough magnetic characterization[32]. We first detail the growth procedure, then analyze the topography and facets of the dots, and finally examine their zero-field magnetization configuration, revealing the occurrence of a single magnetic vortex. Prior to this report, we used these dots to study the dimensionality cross-over between a magnetic domain wall and a magnetic vortex[33].

Epitaxial growth was conducted using pulsed-laser deposition in a set of ultra-high vacuum chambers described elsewhere[22]. The laser is a doubled Nd-YAG ($\lambda = 532\,\mathrm{nm}$) with a pulse length of the order of 25 ns. Atomic force microscopy (AFM) and Magnetic force microscopy (MFM) were performed with a NT-MDT Ntegra microscope operated under atmospheric pressure, using either Asylum MFM probes based on AC240TS Olympus cantilevers, or ultrasharp SSS-PPP-MFMR probes from Nanosensors. The MFM signal consists of the phase, with the convention of dark (resp. bright) contrast indicative of attractive (resp. repulsive) forces. Lorentz Microscopy was performed on a FEI Titan 80-300 fitted with a Lorentz lens and a Gatan Imaging filter. The sample was prepared using mechanical polishing and

*Olivier.Fruchart@grenoble.cnrs.fr
†Present address: CEMES, 29 rue Jeanne Marvig, 31055 Toulouse, France

ion milling. Magnetic information is gained in out-of-focus conditions, where bright and dark Fresnel contrast arise from the overlapping (resp. spreading) of electrons experiencing different Lorentz forces in neighboring domains. Fresnel contrast thus highlights strong magnetization gradients, such as magnetic domain walls and vortices. Micromagnetic simulations were performed using feellgood, a home-built code based on the temporal integration of the Landau-Lifshitz-Gilbert equation in a finite element scheme, *i.e.* using tetrahedra to discretize the dots[34]. Only exchange and magnetostatic interactions were taken into account, to deal with the present case of magnetically-soft dots. The parameters for bulk cobalt were used: $A = 3 \times 10^{-11}\,\mathrm{J/m}$ and $\mu_0 M_\mathrm{s} = 1.7844\,\mathrm{T}$. The tetrahedron size was 4 nm on the average, smaller than the dipolar exchange length of Co $\Delta_\mathrm{d} = 5\,\mathrm{nm}$.

II. GROWTH AND STRUCTURE

We start from a Sapphire $(11\bar{2}0)$ wafer outgassed under UHV. All materials are then evaporated at a rate close to 1 Å/min. We first deposit 0.7 nm of Mo followed by 10 nm of W at 150 °C. A smooth and single-crystalline W(110) surface results from annealing this stack at 900 °C[22]. Reflection high energy electron diffraction (RHEED) shows patterns with very narrow peaks perpendicular to the sample surface, indicating the good crystalline quality of this buffer layer (FIG. 1a). Scanning tunneling microscopy confirms the flatness of the layer, displaying terraces of width several hundreds of nanometers.

Co is then deposited on this surface at 400 °C, with a nominal thickness of several nanometers. RHEED patterns are invariant upon rotation of the sample by 60°, which hints at the occurrence of a growth direction either hexagonal (0001), or fcc (111). These directions of growth are expected as associated with the densest planes of Co, with a triangular symmetry nearly matching in symmetry and dimensions those of body-centered cubic W(110)[35]. The analysis of the RHEED inter-streak distances is consistent with such triangular planes for bulk Co. The absence of $\approx \pm 2.5°$ twins is indicative of the Nishiyama-Wasserman epitaxial relationship[36, 37], for which two sides of the hexagons in the Co planes are parallel to the short side of the rectangular surface lattice of W.

The most stable cristalline structure of bulk Co is hcp below 425 °C, and fcc above this temperature. Due to an elevated temperature and stress related to low dimensions, fcc Co is often found in nanostructures and thin films. The hcp, fcc and even bcc[38] lattices may be selected depending on the chemical nature and orientation of the supporting surface. Let us examine in further detail the RHEED patterns of the deposit to determine its cristalline structure in our case. While patterns along the azimuth W[110] (modulo 60°) display only streaks perpendicular to the sample surface, patterns for the

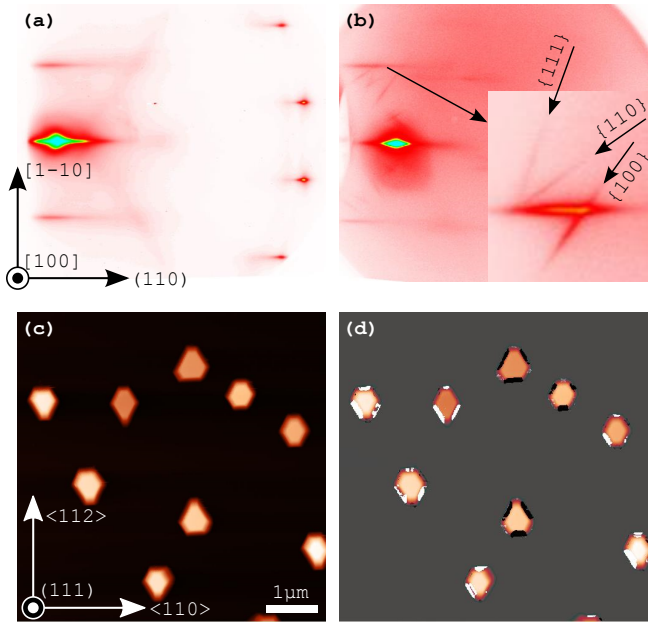

FIG. 1: (a) RHEED pattern of the W(110) supporting surface with beam azimuth [100] (b) RHEED on Co dots along the same azimuth. The inset is a zoom around the first-order streak, with a change of azimuth of a few degrees to better highlight the tilted streaks related to the facets. The angle of the arrows is not a fit to the streaks, but is set *a priori* to that for fcc planes (c) AFM image of Co dots. (d) Same as before, with the 100 facets highlighted in two sets depending on their azimuth: 0°, 120° and 240° (black); 60°, 180° and 300° (white).

beam azimuth along the W[001] direction display those streaks, plus a set of streaks tilted at several well-defined angles (FIG. 1b). This hints at the occurrence of dots of large size, with a flat top and atomically-flat tilted facets[22]. The set of angles deduced from these patterns is consistent with those expected for low-Miller-index planes of a fcc crystal (see Annex for details, including FIG. 6). To the contrary (calculations not provided here), these angles canot be reproduced based on an hcp structure. This strongly suggests that Co grows with a fcc lattice. The epitaxial relationship is thus written: Co(111)//W(110). While the occurrence of the fcc phase is not surprising due first to the low dimension (usually favoring fcc Co), second to the fact that the stable form of Co at the growth temperature is fcc. Nevertheless, we will see in the magnetics part that in practice a very small fraction of dots also grows in the hcp structure. These facts are consistent with a report of the growth of Co at elevated temperature on Mg0(001), also yielding self-assembled dots mostly with an fcc structure, in that case with a (001) top facet, and a minority with an hcp structure[32].

Characterization in real space using AFM in shown in FIG. 1c. The density of the dots is of the order of $0.25\,\mu\mathrm{m}^{-1}$. Like for the case of Fe(110) dots, this den-

sity is mostly determined by temperature during deposition, while the thickness of the deposit affects primarily the volume of the dots. AFM confirms the smoothness of both the top surface and side facets. Figures for the tilt of the latter are consistent with those deduced from RHEED (FIG. 2). The facet analysis (FIG. 1d) shows that the invariance upon rotation of 60° results from the coexistence of two sets of dots, rotated with each other by 180°. This twinned epitaxial relationship is expected and observed for the fcc(111)/bcc(110) Nishiyama-Wasserman epitaxy. FIG. 2 shows a sketch of a typical Co(111) dot resulting from RHEED and AFM data.

The shape of crystals at surfaces is determined by the Wulff-Kaishev construction[39], stating that:

$$\frac{\gamma_i}{h_i} = \frac{(\gamma_S - \gamma_{int})}{h_{int}} = \text{Constant} \qquad (1)$$

h_i is the distance from the (possibly hypothetical) center of the crystal to a given set of crystallographic planes of the material (the facets), γ_i is the free energy of facet i, γ_S is that of the free surface of the substrate, γ_{int} is the interfacial free energy[39] (defined as zero for a material in contact with itself), and h_{int} is a distance related to the vertical aspect ratio of the supported crystal (FIG. 2a). Thus ratios of surface and interface energies may be determined from the observed shape of a crystal. We consider as unknowns $\Delta\gamma = \gamma_S - \gamma_{int}$, and the energy of the facets identified with RHEED and AFM: γ_{111}, γ_{110} and γ_{100}. Notice that another choice instead of $\Delta\gamma$ would be to use the adhesion energy $\gamma^* = \gamma_{111} + \gamma_S - \gamma_{int}$[31].

Only ratios may be determined, which leaves three dimensionless unknowns. Three experimental geometrical ratios are required to determine these three figures, see appendix II. Based on the analysis of all dots on FIG. 1a we find $\Delta\gamma = (0.41 \pm 0.11)\gamma_{111}$, $\gamma_{110} = (1.06 \pm 0.04)\gamma_{111}$ and $\gamma_{100} = (0.88 \pm 0.07)\gamma_{111}$. The error figures stand for the standard deviation. The larger energy for {111} and {110} surfaces than for {100} surfaces is responsible for the triangular shape of our nanocrystals, with the former facets of smaller extent than the latter. Notice also the larger standard deviation for the value of $\Delta\gamma$. This is consistent with the sensitivity of adhesion energy on adsorbates such as resulting from residual gas[22]. In the present case very flat fcc Co platelets may be obtained under poor vacuum conditions (FIG. 5a).

Let us compare the above figures for surface energy with data from the literature. Some data were reported for hcp Co, while others pertain to fcc Co. Besides, experimental values are measured at elevated temperature while theoretical ones are often relevant for zero temperature. Thus, a quantitative comparison is difficult. If one were interested in absolute values, and assuming hcp (0001) and fcc (111) planes have similar surface energies, $\gamma_{111} \approx 2.77\,\mathrm{J/m^2}$ based on calculations[40], while experiments suggest $\gamma_{111} \approx 2.53\,\mathrm{J/m^2}$[41, 42]. However here we will cautiously restrict the discussion to energies nor-

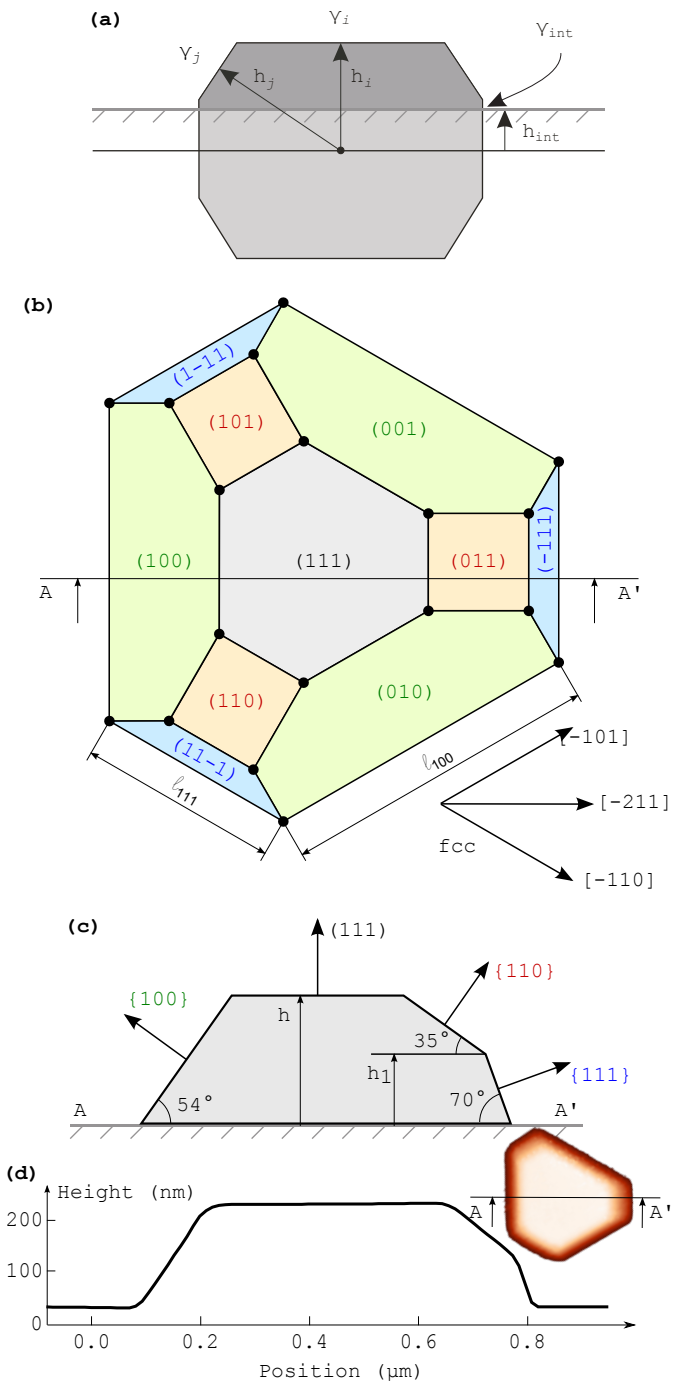

FIG. 2: (a) Wulff-Kaishev construction, and associated notations (b) Top-view schematic of a facetted fcc Co(111) dot. The geometrical ratios are chosen based on the mean values of surface and interface energies determined experimentally (see text). The in-plane lattice directions are shown in the bottom right corner. (c) Schematic and (d) experimental cross-sections. In the latter case the dot used is the one most up in FIG. 1c.

malized with γ_{111} as a reference. There exists no prior quantitative discussion of fcc Co surface energies based on supported nanocrystals. Silly *et al.* [31] simply report the existence of both {111} and {100} facets for Co nanocrystals on $SrTiO_3$(001), and Benamara *et al.* report {111}, {100} and {110} facets for fcc Co(001) dots self-assembled on MgO(001)[32].

It is often argued that surface energy increases for orientations with more open planes, so that we would expect $\gamma_{111} < \gamma_{100} < \gamma_{110}$[43]. Ignoring all details in the anisotropy of the band structure, this is expected as long as non-magnetic materials are considered. However non-zero spin polarization modifies this picture and is for instance responsible for a dip in the magnitude of surface energy towards the center of the $3d$ series, *i.e.* for the strongest value of local moment[44]. A fine point is the following: as magnetic moments at surfaces are modified with respect to the bulk, in a manner that depends on the local coordination[45] and thus of the openness of this surface, the reduction of magnitude depends on the surface considered[46]. It is now recognized theoretically that this causes an anomaly in magnetic materials, where the densest place of atoms is not necessarily associated with the lowest surface energy: $\gamma_{001} < \gamma_{110}$ for bcc Fe[40], and $\gamma_{001} < \gamma_{111}$ for fcc Co[44].

$\Delta\gamma = \gamma_S - \gamma_{int}$ is more difficult to discuss. First, γ_S is not a value known *a priori* from bulk properties like γ_i, as it is the surface energy of a monolayer of pseudomorphic Co wetting the W(110) surface. Second, γ_{int} results not only from electronic contributions expected to be weak in the case of a Stranski-Krastanov growth mode, however also from strain energy related to the accommodation of lattice misfit between the two elements. Nevertheless, assuming γ_S to be similar to γ_{111}, provides a large value for the interfacial energy: $\gamma_{int} \approx 0.6\gamma_{111}$, probably of primarily elastic origin.

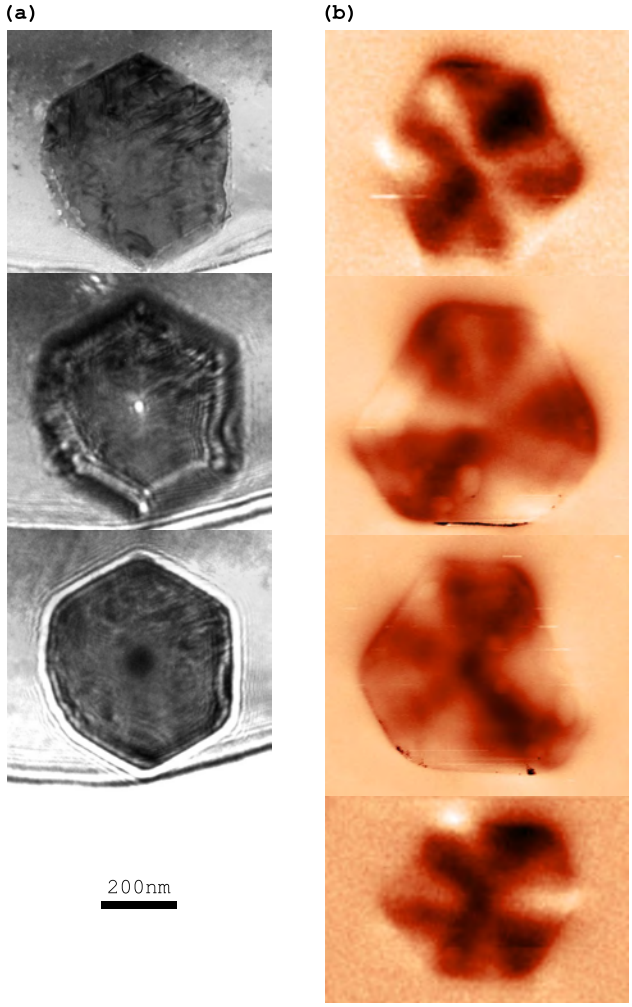

FIG. 3: (a) Lorentz microscopy of an fcc Co dot. From top to bottom: in focus (structure only), over-focused and under-focused. (b) Magnetic Force Microscopy of several fcc Co dots. From top to bottom: vortex up and counter-clock wise (up-CCW), up-CW, down-CCW, down-CW.

III. MICROMAGNETIC CONFIGURATIONS

As fcc Co is a rather soft magnetic material, the critical single-domain size[47, 48] is a few times the dipolar exchange length, $\Delta_d \approx 5\,\text{nm}$ for Co. The dots considered here have dimensions much above this, and are thus expected to display a flux-closure configuration. What type of pattern is formed is revealed with magnetic microscopy. We imaged the dots in the as-grown state with Lorentz and Magnetic Force Microscopy (FIG. 3). Whereas elongated dots of sufficient lateral size and thickness break into mainly two domains separated by a Bloch domain wall[24], here the contrast has a higher symmetry.

Lorentz microscopy unambiguously reveals the existence of a magnetic vortex at the center of the dot. The bright (or dark) contrast in over (or under) focal settings results from the opposite sign of the Lorentz force on either side of the vortex. This contrast informs us about the in-plane circulation of the flux closure, however not about the polarity of the vortex, *i.e.* the sign of the vertical component of magnetization in its core. A strength of Lorentz microscopy is its high spatial resolution, which we used on such dots to investigate the dimensionality cross-over from a vortex to a Bloch wall[33].

On the reverse, MFM is well suited to determine the polarity of the vortex. An up or down polarity is associated with opposite signs of the stray field above the dot, inducing a bright or dark monopolar contrast at the center of the dot (FIG. 3b). The contrast outside the vortex core is related to small-angle Néel walls, which give rise to a dipolar contrast. The sense of this contrast provides information about the in-plane circulation of magnetization around the core. The two degrees of freedom, core polarity and in-plane circulation, are independent (FIG. 3b). Those features are reproduced by micromagnetic simulations (FIG. 4). In addition, in the

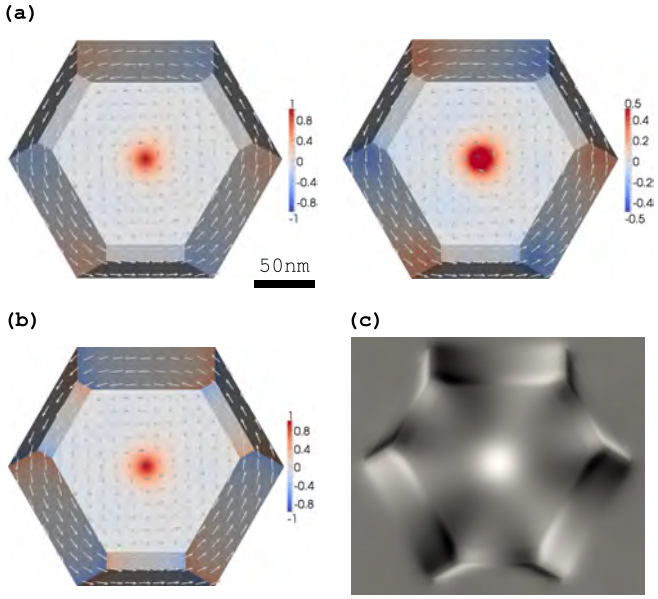

FIG. 4: Micromagnetic simulations of an fcc Co(111) dot of thickness 50 nm. (a) Distribution of magnetization, with color coding the perpendicular component of surface magnetization, while the luminance revels the facets. Two ranges of colors are shown, suited to either the vortex, or the side facets. (b) The color codes the surface charges (c) Simulated MFM contrast: first order vertical derivative of the vertical component of stray field, calculated 10 nm above the surface of the dot.

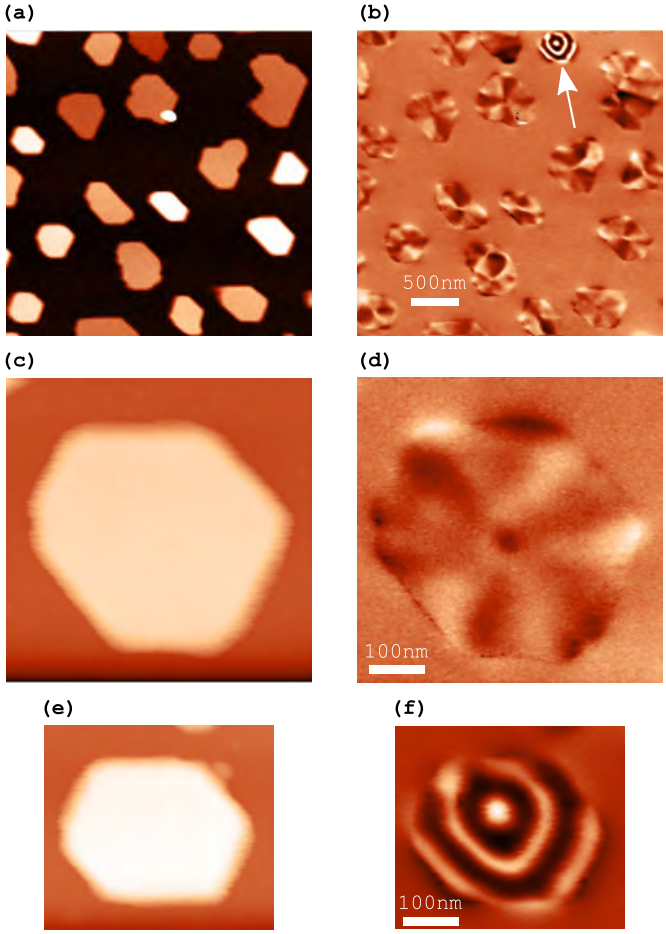

FIG. 5: Co dots with a flat aspect ratio, and height in the range [30−60 nm]. Large scale view of (a) topography and (b) MFM contrast. On the latter the white arrow highlights a dot with hcp lattice. (c-d) Zoom of a fcc dot with height 33 nm (e-f) Zoom of the hcp dot highlighted in (b), with height 25 nm.

experiments the MFM contrast is shifted towards darker values, due to the so-called susceptibility contrast resulting from the softness of sample and/or tip[49].

Let us notice a finer point. As magnetization remains mainly in-plane at the perimeter, the occurrence of surface charges cannot be avoided on the facets around the tilted edges (FIG. 4b). This gives rise to a sharp MFM contrast close to those edges. Due to the three-fold symmetry of the facets (inclination and difference of area on opposite sides), this contributes to the emergence of a three-fold symmetry of the contrast. While this is clear in the simulations, in the experiments it requires more attention due to the somewhat irregular shape. It is more marked for thicker dots as in FIG. 3b where dipolar effects are more important.

We finally report special cases of self-assembled Co(111) dots. A first case is that of dots grown under poor vacuum conditions, which we already mentioned are much flatter than those reported above (FIG. 5). For these the MFM contrast is sharper as the stray field is shorter-ranged. Although the signal over noise ratio is degraded, this decreases the contrast arising from the Néel walls and thus makes the inspection of the vortex core much easier than for thicker dots. A second case is dots with an hcp structure. Both Lorentz and MFM revealed a small fraction of dots with a drastically different distribution of magnetization with abundance of a few percent (FIG. 5a-b;e-f), be they grown under high or poor vacuum conditions. This pattern is typical for stripe-domain phases, as found in materials with a bulk magneto-crystalline contribution to perpendicular magnetic anisotropy[50–53]. In the case of finite-size systems the stripes tend to follow the edges and form a ring structure[54]. This view of local perpendicular magnetization is confirmed by the MFM contrast being much larger on such dots than on in-plane flux-closure ones. This suggests that these dots are hcp Co with the c axis perpendicular to the supporting surface. AFM confirms this, as the facets of such dots show a six-fold symmetry with an inclination of $\approx 30°$, consistent with hcp$\{10-13\}$ facets.

To conclude, we used pulsed laser deposition to synthesize submicrometer Co fcc single crystals supported on a W(110)/Sapphire surface. From the analysis of the geometry of the dots we deduced the ratios of surface and interface energies of fcc Co. $\{111\}$ surfaces have an

energy more than ten percents higher than {100} ones, resulting from the magnetic anomaly in surface energy. These dots form a flux-closure vortex state with an in-plane circulation of magnetization, suitable for studying vortex physics in a model system with no crystalline defects nor surface roughness.

Appendix I

We calculate the inclination angles θ (with respect to the substrate plane) of the major possible facets of fcc(111) dots. We index facets with respect to their normal in the cubic reciprocal lattice: $\mathbf{q} = h\mathbf{a}^* + k\mathbf{b}^* + l\mathbf{c}^*$. As only angles matter here, for simplicity we release the fcc constraint that h, k and l should be of same parity. FIG. 6 shows the directions of atomic rows in the fcc lattice, and notations for the calculation. In the experiments facets only occur with <110> as the direction of the base, so that we restrict the calculation to this case. In the following we consider $[-110]$ as the base atomic row, with no loss of generality. All facets obey $\mathbf{q}.[-110] = 0$ and $\mathbf{q}.[111] \geq 0$, implying $k = h$ and $l \geq -2h$. The facet angle then reads:

$$\cos\theta = \frac{2h + l}{\sqrt{3}\sqrt{2h^2 + l^2}} \tag{2}$$

As facets on opposite sides are different due to the ABC stacking (see FIG. 6a), we must distinguish the two cases: $\mathbf{h}_1.[11-2] \geq 0$ and $\mathbf{h}_2.[-1-12] \geq 0$, implying $l \geq h$ and $l \leq h$, respectively. The main facets are listed in FIG. 6b.

Appendix II

Here we provide relationships between the shape of a supported fcc(111) crystal and ratios of surface/interface energies. Using the notations illustrated in FIG. 2 simple algebra yields geometrical ratios determined by surface/interface energies:

$$\frac{h}{w} = \frac{1 - \Delta\gamma}{\frac{3}{2\sqrt{2}}(1 - \Delta\gamma) + \sqrt{\frac{3}{2}}\gamma_{100}} \tag{3}$$

$$\frac{h_1}{h} = \frac{2\sqrt{\frac{2}{3}}\gamma_{110} - 1 - \Delta\gamma}{1 - \Delta\gamma} \tag{4}$$

$$\frac{\ell_{111}}{\ell_{100}} = \frac{2\sqrt{2}\gamma_{100} - \sqrt{\frac{3}{2}}(\Delta\gamma + 1)}{\sqrt{2}(\sqrt{3} - \gamma_{100})}. \tag{5}$$

Alternatively and of interest in the present case, the determination of surface/interface energies from geometrical ratios of the crystal:

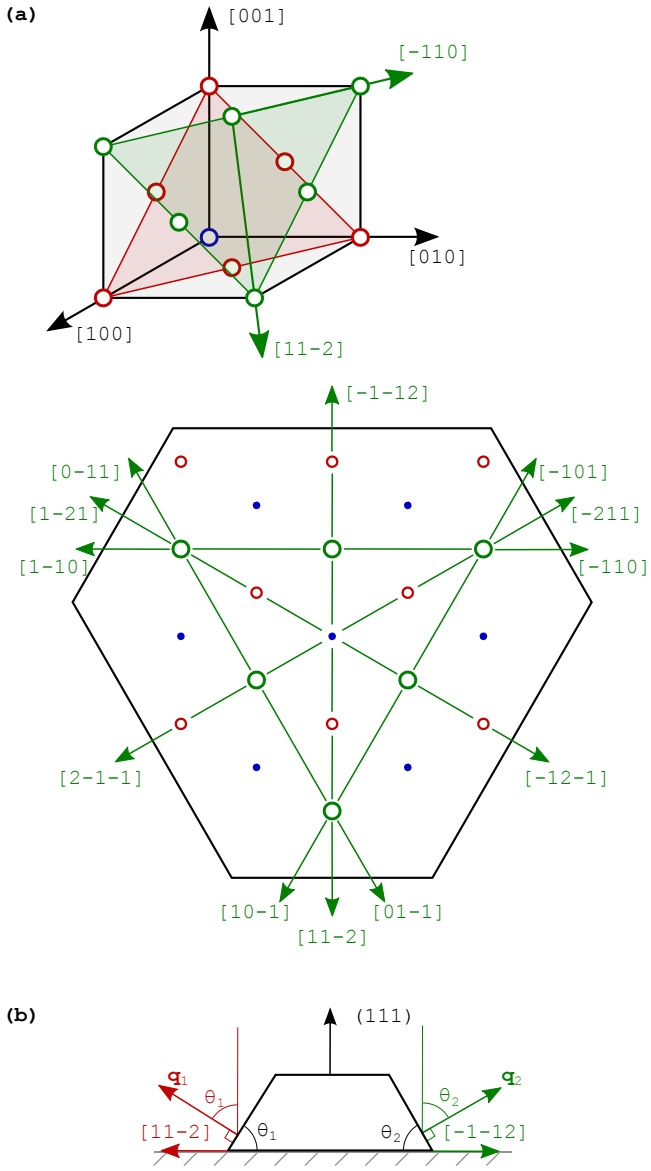

l \ h	-1	0	1	2	3
3	(-1-13) 79.98°	(001) 54.74°	(113) 29.50°	(112) 11.42°	(111) 0°
2	(-1-12) 90°	(001) 54.74°	(112) 19.47°	(111) 0°	(332) 10.02°
1		**(001) 54.74°**	**(111) 0°**	(221) 15.79°	(332) 22.00°
0			**(110) 35.26°**	(110) 35.26°	(110) 35.26°
-1			**(11-1) 70.53°**	(22-1) 54.74°	(33-1) 48.53°
-2			(11-2) 90°	(11-1) 70.53°	(33-2) 60.50°
-3				(22-3) 70.53°	(11-1) 70.53°

FIG. 6: (a) Stacking of planes and directions of atomic rows for the fcc lattice. (b) Notations for the identification of facets, and list of the main facets. Those observed experimentally are highlighted with bold figures.

$$\gamma_{100} = \sqrt{3}\left[1 - \frac{1}{\left(1+\frac{\ell_{111}}{\ell_{100}}\right)\left(1-\frac{h}{w}\frac{3}{2\sqrt{2}}\right)+1}\right] \quad (6)$$

$$\gamma_{110} = \sqrt{\frac{3}{2}}\left[1 - \frac{3}{2\sqrt{2}}\frac{h}{w}\frac{\left(1+\frac{\ell_{111}}{\ell_{100}}\right)\left(1-\frac{h_1}{h}\right)}{\left(1+\frac{\ell_{111}}{\ell_{100}}\right)\left(1-\frac{h}{w}\frac{3}{2\sqrt{2}}\right)+1}\right] \quad (7)$$

$$\Delta\gamma = 1 - \frac{3}{\sqrt{2}}\frac{h}{w}\frac{1+\frac{\ell_{111}}{\ell_{100}}}{\left(1+\frac{\ell_{111}}{\ell_{100}}\right)\left(1-\frac{h}{w}\frac{3}{2\sqrt{2}}\right)+1}. \quad (8)$$

Acknowledgments

We acknowledge useful discussions with O. Benamara (Cemes, Toulouse, France), V. Dupuis (LPMCN, Lyon, France), R. Morel (INAC, Grenoble, France) and technical help from A. Rousseau, Z. Kassir-Bodon, Ph. David and V. Guisset. This work was partly conducted as practicals for students, funded by Grenoble Institute of Technology (G-INP). We acknowledge financial support from European FP6 EU-NSF program (STRP 016447 MagDot).

References

[1] H. Masuda and H. Fukuda, Science **268**, 1466 (1995).
[2] W. Lee, R. Ji, U. Gösele, and K. Nielsch, Nat. Mater. **5**, 741 (2006).
[3] W. Lee and J.-C. Kim, Nanotechnology **21**, 485304 (2010).
[4] M. Knez, K. Nielsch, and L. Niinistö, Adv. Mater. **19**, 3425 (2007).
[5] P. W. Rothemund, Nature **440**, 297 (2006).
[6] P. Gambardella, A. Dallmeyer, K. Maiti, M. C. Malagoli, W. Eberhardt, K. Kern, and C. Carbone, Nature **416**, 301 (2002).
[7] J. Bansmann, S. Baker, C. Binns, J. Blackman, J.-P. Bucher, J. Dorantes-DÁvila, V. Dupuis, L. Favre, D. Kechrakos, A. Kleibert, K.-H. Meiwes-Broer, G. M. Pastor, A. Perez, O. Toulemonde, K. N. Trohidou, J. Tuaillon, and Y. Xie, Surf. Sci. Rep. **56**, 189 (2005).
[8] R. Hertel, O. Fruchart, S. Cherifi, P. O. Jubert, S. Heun, A. Locatelli, and J. Kirschner, Phys. Rev. B **72**, 214409 (2005).
[9] A. Enders, R. Skomski, and J. Honolka, J. Phys.: Condens. Matter **22**, 433001 (2010).
[10] A. J. Cox, J. G. Louderback, and L. A. Bloomfield, Phys. Rev. Lett. **71**, 923 (1993).
[11] L. Gerhard, T. K. Yamada, T. Balashov, A. F. Takacs, R. J. H. Wesselink, M. Dane, M.Fechner, S. Ostanin, A. Ernst, I. Mertig, and W. Wulfhekel, IEEE Trans. Magn. **47**, 1619 (2011).
[12] M. Jamet, A. Barski, T. Devillers, V. Poydenot, R. Dujardin, P. Bayle-Guillemaud, J. Rothman, E. Bellet-Amalric, A. Marty, J. Cibert, R. Mattana, and S. Tatarenko, Nat. Mater. **5**, 653 (2006).
[13] F. Vidal, Y. Zheng, J. Milano, D. Demaille, P. Schio, E. Fonda, and B. Vodungbo, Appl. Phys. Lett. **95**, 152510 (2009).
[14] H. Zheng, J. Wang, S. E. Lofland, Z. Ma, L. Mohaddes-Ardabili, T. Zhao, L. Salamanca-Riba, S. R. Shinde, S. B. Ogale, F. Bai, D. Viehland, Y. Jia, D. G. Schlom, M. Wuttig, A. Roytburd, and R. Ramesh, Science **303**, 661 (2004).
[15] A. Fert and J. L. Piraux, J. Magn. Magn. Mater. **200**, 338 (1999).
[16] K. Nielsch, F. Müller, A.-P. Li, and U. Gösele, Adv. Mater. **12**, 582 (2000).
[17] B. Chaudret, C. R. Physique **6**, 117 (2005).
[18] P. O. Jubert, O. Fruchart, and C. Meyer, Phys. Rev. B **64**, 115419 (2001).
[19] O. Fruchart, C. R. Physique **6**, 61 (2005).
[20] R. Zdyb, A. Pavlovska, M. Jalochowski, and E. Bauer, Surf. Sci. **600**, 1586 (2006).
[21] N. Rougemaille and A. K. Schmid, J. Appl. Phys. **99**, 08S502 (2006).
[22] O. Fruchart, P. O. Jubert, M. Eleoui, F. Cheynis, B. Borca, P. David, V. Santonacci, A. Liénard, M. Hasegawa, and C. Meyer, J. Phys.: Condens. Matter **19**, 053001 (2007).
[23] H. A. M. van den Berg, J. Magn. Magn. Mater. **44**, 207 (1984).
[24] P. O. Jubert, J. C. Toussaint, O. Fruchart, C. Meyer, and Y. Samson, Europhys. Lett. **63**, 132 (2003).
[25] F. Cheynis, A. Masseboeuf, O. Fruchart, N. Rougemaille, J. C. Toussaint, R. Belkhou, P. Bayle-Guillemaud, and A. Marty, Phys. Rev. Lett. **102**, 107201 (2009).
[26] O. Fruchart, N. Rougemaille, J. C. Toussaint, R. Belkhou, Y. Tian, H. Yu, F. Cheynis, A. Masseboeuf, P. Bayle-Guillemaud, and A. Marty, IEEE Trans. Magn. **46**, 1552 (2010).
[27] T. Shinjo, T. Okuno, R. Hassdorf, K. Shigeto, and T. Ono, Science **289**, 930 (2000).
[28] B. Van Waeyenberge, A. Puzic, H. Stoll, K. W. Chou, T. Tyliszczak, R. Hertel, M. Fähnle, H. Brückl, K. Rott, G. Reiss, I. Neudecker, D. Weiss, C. H. Back, and G. Schütz, Nature **444**, 461 (2006).
[29] R. Cheng, J. Pearson, H. F. Ding, V. Metlushko, S. D. Bader, F. Y. Fradin, and D. Li, Phys. Rev. B **69**, 184409 (2004).
[30] H. F. Ding, A. K. Schmid, Dongqi Li, K. Yu, K. Yu Guslienko, and S. D. Bader, Phys. Rev. Lett. **94**, 157202 (2005), submitted.
[31] F. Silly and M. R. Castell, Appl. Phys. Lett. **87**, 053106 (2005).
[32] O. Benamara, E. Snoeck, T. Blon, and M. Respaud, J. Cryst. Growth **312**, 1636 (2010).
[33] A. Massebœuf, O. Fruchart, J. C. Toussaint, E. Kritsikis,

L. Buda-Prejbeanu, F. Cheynis, P. Bayle-Guillemaud, and A. Marty, Phys. Rev. Lett. **104**, 127204 (2010).
[34] F. Alouges, E. Kritsikis, and J.-C. Toussaint, Physica B **407**, 1345 (2012).
[35] E. Bauer and J. H. Van der Merwe, Phys. Rev. **B33**, 3657 (1986).
[36] Y. Gotoh and H. Fukuda, Surf. Sci. **223**, 315 (1989).
[37] J. H. van der Merwe, D. L. Tönsing, and P. M. Stoop, Thin Solid Films **237**, 297 (1994).
[38] M. Ohtake, O. Yabuhara, J. Higuchi, and M. Futamoto, J. Appl. Phys. **107**, 07C105 (2011).
[39] C. R. Henry, Prog. Surf. Sci. **80**, 92 (2005).
[40] L. Vitos, A. V. Ruban, H. L. Skiver, and J. Koll'ar, Surf. Sci. **411**, 186 (1998).
[41] A. R. Miedema and B. E. Nieuwenhuys, Surf. Sci. **104**, 491 (1981).
[42] F. R. de Boer, R. Boom, W. C. M. Mattens, A. Miedema, and A. K. Niessen, in Cohesion in Metals, edited by F. R. de Boer and D. G. Pettifor (North-Holland, Amsterdam, 1988), Vol. I, p. 676.
[43] M. Aldén, S. Mirbt, H. L. Skriver, N. M. Rosengaard, and B. Johansson, Phys. Rev. B **46**, 6303 (1992).
[44] M. Aldén, H. L. Skriver, S. Mirbt, and B. Johansson, Surf. Sci. **315**, 157 (1994).
[45] P. Gambardella, S. Rusponi, M. Veronese, S. S. Dhesi, C. Grazioli, A. Dallmeyer, I. Cabria, R. Zeller, P. H. Dederichs, K. Kern, C. Carbone, and H. Brune, Science **300**, 1130 (2003).
[46] M. P. J. Punkkinen, Q.-M. Hu, S. K. Kwon, B. Johansson, J. Kollár, and L. Vitos, Philos. Mag. **91**, 3627 (2011).
[47] A. Hubert and R. Schäfer, Magnetic domains. The analysis of magnetic microstructures (Springer, Berlin, 1999), .
[48] O. Fruchart and A. Thiaville, C. R. Physique **6**, 921 (2005).
[49] D. W. Abraham and F. A. McDonald, Appl. Phys. Lett. **56**, 1181 (1990).
[50] C. Kittel, Phys. Rev. **70**, 965 (1946).
[51] Z. Malek and V. Kambersky, Czechols. J. Phys. **8**, 416 (1958).
[52] Y. Murayama, J. Phys. Soc. Jap. **21**, 2253 (1966).
[53] Y. Murayama, J. Phys. Soc. Jap. **23**, 510 (1967).
[54] M. Hehn, K. Ounadjela, J. P. Bucher, F. Rousseaux, D. Decanini, B. Bartenlian, and C. Chappert, Science **272**, 1782 (1996).